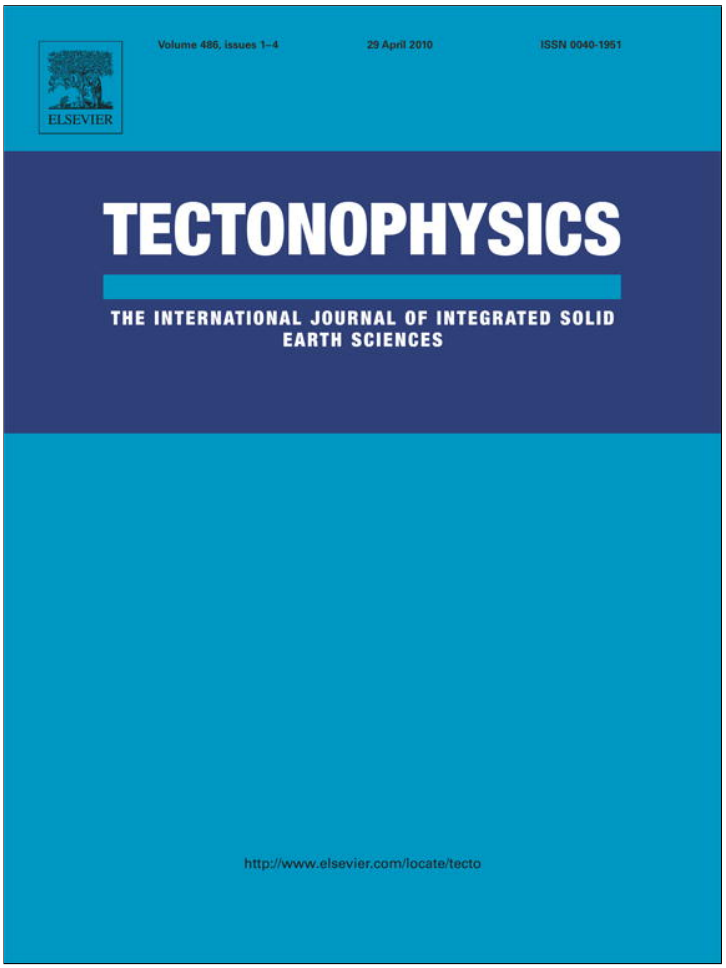

Tectonophysics 486 (2010) 120–131

Contents lists available at ScienceDirect

Tectonophysics

journal homepage: www.elsevier.com/locate/tecto

Correlation between the anisotropy of the magnetic susceptibility, strain and X-ray Texture Goniometry in phyllites from Crete, Greece

Belén Oliva-Urcia [a,*], Jeffrey M. Rahl [b], Anja M. Schleicher [a], Josep M. Parés [a,c]

[a] University of Michigan, 1100 North University Avenue, Ann Arbor, 48106 MI, United States
[b] Department of Geology, Washington and Lee University, Lexington, VA 24450, United States
[c] CENIEH-Centro Nacional sobre la investigación humana, Avda. de la Paz, 28, 09004 Burgos, Spain

ARTICLE INFO

Article history:
Received 21 July 2009
Received in revised form 2 February 2010
Accepted 19 February 2010
Available online 26 February 2010

Keywords:
AMS
PDS
XTG
SMT
Crete

ABSTRACT

A comparison of petrofabric and strain in phyllitic rocks from Crete, Greece has been undertaken using Anisotropy of Magnetic Susceptibility (AMS) at room and low temperature, the Projected Dimension Strain method (PDS), and X-ray Texture Goniometry (XTG) of phyllosilicates. The magnetic (at room and low temperature) and strain fabrics show similar orientations, with the minimum axes of the AMS ellipsoid coincident with the flattening direction of a pronounced solution mass-transfer deformation (SMT). The k_{max} axes of the AMS and the maximum stretching axis of the deformation overlap in the NNE–SSW direction, parallel to the axes of macroscopic folds. The quantitative relationship between the absolute values of strain and AMS is unclear. Nevertheless, a degree of correlation is found between the Woodcock diagram values of AMS and strain. S_x values discriminate better the clustered samples of k_{max} whereas the girdled samples of k_{max} are better differentiated with the S_z values. The stacking of the octahedral layers in micas correlates with S_x in the clustered k_{max} axes fabrics. The lack of a clear quantitative relationship is probably related to the generation of new phyllosilicates during folding and SMT deformation.

1. Introduction

Since early work with Anisotropy of Magnetic Susceptibility (AMS) measurements at low field (e.g., Graham, 1954), a principal aim of magnetic fabric studies has been to relate the magnetic ellipsoid with the petrofabric of deformed rocks (Rees, 1965; Graham, 1966; Borradaile and Tarling, 1981; Borradaile and Jackson, 2004). If the relationship between the magnetic ellipsoid and the strain ellipsoid is well-understood, AMS represents a valuable tool to measure finite strain in deformed rocks in a relatively fast and non-destructive manner (Goldstein, 1980; Rathore, 1980; Kligfield et al., 1981, 1982; Hrouda, 1982; Borradaile, 1987; Lowrie, 1989; Borradaile, 1991; Jackson and Tauxe, 1991; Rochette et al., 1992; Hirt et al., 1993; Tarling and Hrouda, 1993; Averbuch et al., 1995; Housen et al., 1995; Borradaile and Henry, 1997; Lüneburg et al., 1999; Parés and van der Pluijm, 2002, Anderson and Morris, 2004). Although previous studies have documented that the orientations of the magnetic and strain ellipsoids are generally similar (Kneen, 1976; Wood et al., 1976; Kligfield et al., 1977; Rathore, 1979; Kligfield et al., 1982; Rathore and Henry, 1982; Lüneburg et al., 1999), their magnitudes are more complexly related and a clear empirical relationship has yet to be established for all lithologies (Kligfield et al., 1981; Borradaile, 1987, 1988; Hirt et al., 1988; Borradaile, 1991; Lüneburg et al., 1999). However, the shape magnetic parameter (T) has been shown to be a good indicator of the deformation intensity in slates that experienced a low-to-moderate degree of deformation (Parés and van der Pluijm, 2003 and references therein).

The AMS ellipsoid is primarily sensitive to the degree of alignment of each contributing mineral phase (paramagnetic, ferromagnetic and diamagnetic). Consequently, the relationship between AMS and strain is strongly affected by sample mineralogy, such as the abundance of ferromagnetic grains (like magnetite, with high susceptibility values) or diamagnetic minerals (including quartz and calcite) (Henry and Daly, 1983; Borradaile, 1987; Hrouda, 1987; Rochette, 1987; Borradaile, 1988; Borradaile and Sarvas, 1990; Housen and van der Pluijm, 1990; Jackson, 1991; Hirt et al., 2004). Deformation processes, including grain rotation, grain sliding, kinking or new crystallization of grains, may affect an entire rock or only certain magnetic carriers. Therefore, the development of the magnetic subfabrics (paramagnetic, ferromagnetic and diamagnetic separately) may occur at different times in the history of a rock that experiences evolving deformational and metamorphic conditions. For example, shear related to thrust movement seems to affect remagnetized ferromagnetic grains, with k_{max} axes following the thrust transport direction within the bedding plane, whereas the AMS ellipsoid orientation follows the intersection lineation which in turn is related to either the stretching direction or to the crenulation of platy minerals such as phyllosilicates (Aubourg et al., 1995, 1997, 1999; Aubourg and Chabert-Pelline, 1999). Different generations of white mica and chlorite

* Corresponding author. Universidad de Zaragoza, C/Pedro Cerbuna 12, 50009 Zaragoza, Spain.
E-mail address: boliva@unizar.es (B. Oliva-Urcia).

0040-1951/$ – see front matter © 2010 Elsevier B.V. All rights reserved.
doi:10.1016/j.tecto.2010.02.013

produce a mixed magnetic fabric between bedding and cleavage that cannot be used as strain gauge (Debacker et al., 2004), and chlorite crystallization related to cleavage development results in a "tectonic" fabric with the k_{min} at the pole of the cleavage planes (Housen et al., 1993; Hirt et al., 2004). Thus, an observed AMS ellipsoid reflects the integrated history of deformation. This complicated pattern can only be unraveled with detailed knowledge of the mineralogy and deformational processes that have affected a sample.

In this work we investigate the relationship between the magnetic fabric ellipsoid (at room and low temperature) and the strain ellipsoid in siliciclastic rocks from Crete. Here, solution mass-transfer deformation has resulted in a widespread, sub-horizontal cleavage. The measurements obtained with the Projected Dimension Strain (PDS) method (Feehan and Brandon, 1999; Ring and Brandon, 1999) reflect the strain developed during solution mass-transfer (SMT) deformation, whereas AMS measures the orientation distribution of all grains (detrital and newly-formed) post-deformation. In addition, high-resolution X-ray Texture Goniometry (XTG) data provide an absolute quantification of the orientation of the paramagnetic minerals (mostly micas).

2. The Phyllite–Quartzite Unit of Crete

The Phyllite–Quartzite Unit (PQ) of Crete, Greece, is a package of Late Carboniferous to Late Triassic marine siliciclastics with minor limestones, gypsum, and volcanics (Krahl et al., 1983; Dornsiepen et al., 2001) (Fig. 1). During Oligocene subduction of the downgoing African Plate beneath the European margin, these deposits were accreted through underplating at the base of the Hellenic wedge (e.g., Le Pichon and Angelier, 1981; Angelier et al., 1982). The PQ sediments experienced high-pressure, low-temperature (HP–LT) metamorphism event (about 0.8 to 1.0 GPa, 250 to 400 °C) that culminated at about 25 Ma (Theye et al., 1992; Jolivet et al., 1996; Rahl et al., 2005). The subsequent cooling to below 300 °C took place at a pressure of 0.3–0.4 GPa during a first stage of decompression between 24 (at the earliest) and 19 Ma at an average rate in excess of 4 mm/a, followed by a second stage from 0.3 GPa to <0.1 GPa between 19 and 15 Ma with an average rate of less than 2 mm/a (Rahl, 2005).

The phyllites and quartzites of the PQ unit preserve extensive ductile deformation acquired during the HP–LT event and subsequent exhumation (Greiling, 1982; Fassoulas et al., 1994; Jolivet et al., 1996; Stöckhert et al., 1999). Progressive deformation is evident from both field and microscropic observations. On a macro-scale, the PQ unit displays multiple generations of m to km-scale, commonly recumbent tight folds. Boudinage is occasionally present in the fold limbs and associated with chloritoid, recrystallized quartz, and white mica (Greiling, 1982; Stöckhert et al., 1999). A macroscopic stretching lineation often trends N to NE, inferred to be parallel to both the first-generation of fold axes and the inferred direction of plate convergence (Stöckhert et al., 1999). The folds are modified by a pervasive sub-horizontal foliation interpreted to form early in the deformation history during underplating. At a microscopic scale, deformation of detrital quartz is indicated by a strong shape-preferred orientation. Several lines of evidence indicate that SMT was the primary deformation mechanism active in the phyllites that comprise the bulk of the unit (Schwarz and Stöckhert, 1996; Stöckhert et al., 1999; Rahl, 2005). Quartz grains generally show little evidence of internal deformation such as undulose extinction, sub-grain development, or low-angle grain boundaries (Fig. 2), and when such features are present their orientation is random, suggesting inheritance from the source terrane rather than development following deposition (Stöckhert et al., 1999). Quartz *c*-axis data from the phyllites do not reveal a fabric (Schwarz and Stöckhert, 1996), further indicating that intracrystalline processes did not contribute significantly to the deformation. The edges of quartz grains commonly are lined with phyllosilicates that appear to have facilitated dissolution, and quartz–mica fibers commonly mantle the edge of the detrital grains, oriented parallel to the extension direction within the rock (Fig. 2). The bedding and cleavage planes are sub-parallel and near to the horizontal in all sampled sites.

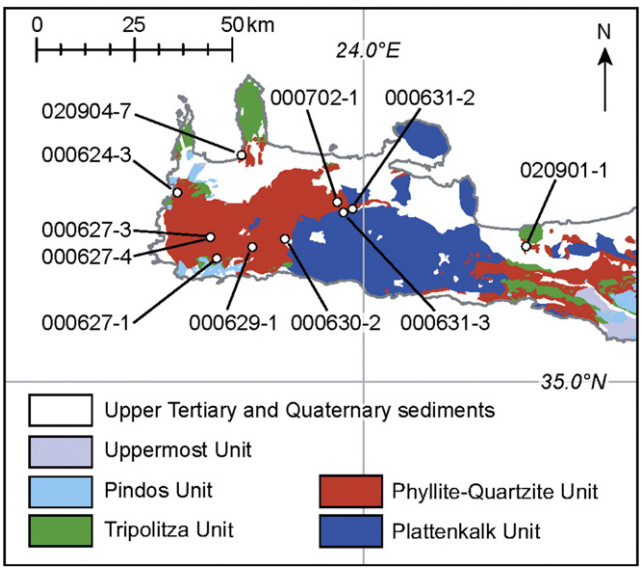

Fig. 1. Simplified geologic map and tectonostratigraphy of Crete, after Rahl et al. (2005).

3. Methods

3.1. Magnetic susceptibility

3.1.1. Carriers

The measurement of the bulk magnetic susceptibility at low temperature (down to liquid nitrogen, i.e.: 77 K) helps to determine the role of paramagnetic phases (Richter and van der Pluijm, 1994). The paramagnetic susceptibility K_p (largely due to phyllosilicates in phyllites) increases linearly with decreasing temperature (T) according to the Curie–Weiss law: $K_p = C/(T-\phi)$, where C is a constant and ϕ is the paramagnetic Curie temperature. Thus, the temperature dependence of susceptibility allows the identification of paramagnetic minerals when these grains are the main carrier of the fabric.

3.1.2. AMS

Magnetic susceptibility is a physical property of solids and represents the capacity of the material to be magnetized in a given

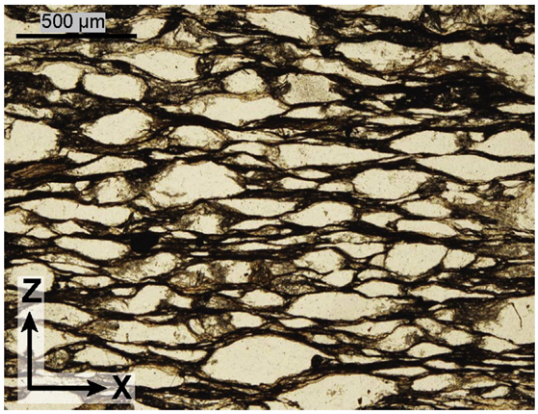

Fig. 2. Plane-light photomicrograph of a representative sample from the Phyllite–Quartzite unit. Section is oriented in the *X–Z* plane (perpendicular to the macroscopic foliation). Detrital quartz grains are internally undeformed but still show a prominent shape-preferred orientation. Insoluble micaceous selvages are often associated with parts of truncated grains. Fibrous overgrowths of quartz and subordinate white mica are straight and parallel to the extension direction.

magnetic field. The magnetic susceptibility (K_m) is described as a symmetric second-rank tensor that relates the applied magnetic field (H) to an induced magnetization (M): $M = K \times H$. This property is anisotropic (Nye, 1957). The anisotropy of magnetic susceptibility (AMS) in rocks depends primarily on crystallographic preferred orientation, shape fabric of grains, composition and magnetic interactions between grains (Tarling and Hrouda, 1993). Three axes define the susceptibility ellipsoid: maximum (k_{max}), intermediate (k_{int}) and minimum (k_{min}). The orientations of these axes correspond to the eigenvectors of the susceptibility tensor. Other parameters that contain information about the shape and degree of magnetic fabric development are: the magnetic lineation ($L = k_{max}/k_{int}$), magnetic foliation ($F = k_{int}/k_{min}$). Following Jelinek (1981), the corrected anisotropy degree, P', shows the intensity of the preferred orientation of minerals; the shape parameter T varies between −1 and +1, with $T<0$ for prolate shapes and $T>0$ for oblate ellipsoids. The principal axes of the ellipsoid are displayed on a stereographic equal area projection to compare with the axes of the strain ellipsoid. The clustering of the k_{max} axes is quantified and shown in the Woodcock diagram, which displays the relationships between the eigenvalues for every axis (Woodcock, 1977). This diagram allows us to distinguish between girdle or cluster distributions for a chosen axis. The grouping of the chosen axis at each site is defined by three eigenvalues and three eigenvectors. The three eigenvalues (e1>e2>e3) sum to 1, and their logarithmic relationship is expressed in the Woodcock diagram, with L_w being the "Woodcock lineation" ($L_w = \mathrm{Ln}(e1/e2)$) and F_w the "Woodcock foliation" ($F_w = \mathrm{Ln}(e2/e3)$). C values are a measurement of the strength of the preferred orientation. For more details see Parés et al. (1999) and Larrasoaña et al. (2004).

A total of 11 sites were investigated for the study of the AMS. All measurements (8 to 10 standard specimens per site) were performed on a susceptibility bridge, Kappabridge KLY-2.03 (Geofyzika Brno) at the University of Michigan, by measuring 15 directional susceptibilities with a frequency of 920 Hz. The sensitivity of the coil is about 5×10^{-7} SI. The data reduction process for each individual sample is as follows: first the matrix elements and individual errors are calculated following Jelinek (1978). AMS measurements give the orientations and magnitudes of the $k_{min} \leq k_{int} \leq k_{max}$ axes of the AMS ellipsoid. Second, the bootstrap statistics for the matrix elements are calculated (Tauxe, 1998).

Low-temperature AMS (LT-AMS) analyses to separate the paramagnetic fabric were performed at the Magnetic Laboratory of the University of Zaragoza. The samples of four sites (2 sites from the girdle distribution and 2 sites from the cluster distribution of k_{max} axes) were immersed in liquid nitrogen (77 K) 1 h before starting the procedure. The apparatus used for the measurements is a KLY3S (AGICO company) in spinning mode. The samples were measured in air, but between the 3 different positions the samples were immersed again in liquid nitrogen for about 10 min (as in Lüneburg et al., 1999). Each of the three positions measured in rotation mode takes about 10–20 s. The AMS determined by this measurement protocol was repeatable.

Because paramagnetic minerals follow the Curie–Weiss law ($K_p = C/T - \theta$) at low temperatures, such measurements enable estimation of paramagnetic AMS. This approach produces a magnetic susceptibility intensity approximately 3.8 times higher than at room temperature (298/77), assuming purely paramagnetic phases with paramagnetic Curie temperature around 0 K (Lüneburg et al., 1999). The increase of the AMS axes is not symmetric at low temperature: the k_{max} axes increase by a factor larger than the k_{min} (Parés and van der Pluijm, 2002). The measurements of AMS at low temperature also provide the orientations and magnitudes of the $k_{min} \leq k_{int} \leq k_{max}$ axes of the AMS ellipsoid that can be compared results obtained at room temperature.

The partial anhysteretic remanent magnetization (pARM) is acquired when a sample is placed in a large alternating field (AF) with decaying amplitude, in the absence of a DC bias field; the bias field is switched on when the AF amplitude reaches a value H_1, and switched off again when the amplitude has decayed to H_2; the AF then decays to zero with no bias field. This procedure magnetizes the population of particles with remanent coercivities between H_1 and H_2, while randomizing the moments of the other particles (Jackson, 1991). $H_2 = H_1 + 10$ mT and the window where the bias field is switched on moves from 0 to 100 mT. The result provides the coercivity spectra of the sample. The measurements in pilot samples from the 11 sites did not produce consistent results, so we discarded the anisotropy of the anhysteretic remanent magnetization (AARM) analyses to separate the ferromagnetic fabric. Nevertheless, the AMS itself provides reliable information about the orientation of minerals to compare directly the AMS ellipsoid with the strain ellipsoid.

3.2. Strain analysis

The microstructures of the PQ unit have been well-characterized but little work has been conducted to determine the magnitude and orientation of strain within the rocks (Schwarz and Stöckhert, 1996; Stöckhert et al., 1999; Rahl, 2005). The Projected Dimension Strain method (PDS, details in Ring and Brandon, 1999 and Rahl, 2005) is applied to quantify deformation within the phyllites of Crete. The PDS method is specifically designed for rocks deformed primarily by SMT. Truncated detrital grains are used to measure pressure-induced shortening by comparing the average grain-dimension parallel to the shortening axis with the average grain-dimension parallel to the extension direction (which remains preserved during SMT deformation). Since extension is accommodated through the precipitation of fibrous overgrowth, extensional stretches were estimated by using the modal abundance of fibrous overgrowth (Feehan and Brandon, 1999). Because the initial grain dimensions are preserved in the direction of extension, the PDS method provides absolute (rather than relative) strain measurements. Samples are analyzed in at least two thin-sections, one within the foliation plane and a second perpendicular to the foliation and parallel to the direction of maximum extension. A detailed description of the methodology and application to these samples is provided in Rahl (2005).

3.3. X-ray Texture Goniometry (XTG) and scanning electron microscopy (SEM)

X-ray Texture Goniometry analysis allows the determination of the crystallographic preferred orientation of phyllosilicates in relatively small regions (ca. 1 mm^2). Oriented samples (200–400 μm thick) were cut perpendicular to the foliation (and bedding) and attached to a glass slide using sticky wax. After polishing, the samples were removed from the slides, glued on aluminum holders and placed in a modified Enraf–Nonious CAD 4 automated single-crystal diffractometer with a molybdenum (Mo) source (alpha = 0.7107 Å) housed in the Electron Microbeam Analytical Laboratory (EMAL) at the University of Michigan.

Following the method of van der Pluijm et al. (1994), bulk X-ray diffraction (XRD) analysis was performed to identify the mineral phases present in the sample. The detector was rotated to the 2θ value corresponding to the Bragg diffraction angle of the 001 and/or 002 plane of phyllosilicates (10 Å for mica, 7 Å for chlorite). Each sample was then rotated and the intensity of the diffracted beam recorded at each of about 1300 positions. The normalized intensity data are expressed in multiples of random distribution (m.r.d. Wenk 1985), a standard statistical measure of the relative randomness of a distribution. When a preferred orientation exists, the diffracted beam intensities cluster, and the intensity of that clustering is a function of the relative perfection of the fabric.

Scanning electron microscopy (SEM) constrains the interpretations of X-ray data by providing images of the mineral assemblages

Table 1
Values from AMS measurements at room temperature. *L*: lineation, *F*: foliation, *P′*: corrected anisotropy degree, *T*: shape parameter and K_m: bulk magnetic susceptibility.

Sample	*L*	*F*	*P′*	*T*	K_m (10^{-6}) SI
000624-3	1.0278	1.0293	1.1258	0.5985	73.5910
000627-1	1.0381	1.1958	1.2605	0.6573	58.4400
000627-3	1.0361	1.1778	1.2373	0.6579	41.5310
000627-4	1.0619	1.1269	1.2005	0.3297	81.1010
000629-1	1.0118	1.0982	1.1224	0.7791	107.5067
000630-2	1.1026	1.2065	1.3418	0.3497	13.0340
000631-2	1.0582	1.1107	1.1813	0.3426	23.9489
000631-3	1.0080	1.1609	1.1939	0.8883	215.3370
000702-1	1.0203	1.0739	1.1013	0.5720	26.8509
020901-1	1.0340	1.1681	1.2238	0.6548	21.7120
020904-7	1.0320	1.1619	1.2141	0.6551	30.8700

and measured fabrics. SEM provides information about the mm to μm scale mineralogical distribution of mineral species within a sample. These data, combined with any crosscutting relationships observed in back-scattered electron (BSE) images, provide information about the mineralization processes and fabric development within the samples. Selected polished samples were cut perpendicular to the cleavage plane and parallel to its dip direction, and were coated with carbon. Back-scattered imaging and semiquantitative analyses of the mineral composition have been obtained using two SEM/EDX systems in the EMAL laboratory (SEM Hitachi S3200N; 20 kV, BSE detector, EDX analyses) at the University of Michigan.

4. Results

4.1. AMS

4.1.1. Carrier of the magnetic fabric

The studied rocks are characterized by a low bulk magnetic susceptibility, with all sites but two having a bulk susceptibility lower than 100×10^{-6} SI (see Table 1). This suggests that the contribution from ferromagnetic grains to the susceptibility is not significant (e.g., Tarling and Hrouda, 1993), although some exceptions have been described in rocks with ferromagnetic content but low bulk susceptibility values (e.g., Hirt et al., 2004). Variation of magnetic susceptibility with temperature curves confirms that paramagnetic minerals (phyllosilicates) represent the main contributors to the magnetic fabric in most samples (Fig. 3A). The linear increase of the reciprocal susceptibility between 200 and 400–600 s (approximately 100–250 K) indicates a predominance of paramagnetic minerals as the carriers of the magnetic fabric. The curves follow the Curie–Weiss law almost perfectly. However, a contribution of a ferromagnetic mineral is detectable in samples 627-4, 702-1 and 629-1 (Fig. 3B). The jump in susceptibility for the three above-mentioned samples at around 200 s may indicate some crystallographic transition (as the one of magnetite at 120 K found in similar experiments by Parés et al., 1999). The abundance of quartz grains lowers the bulk susceptibility at room temperature (K_m) because quartz is a diamagnetic mineral with low crystallographic anisotropy (−14 μm SI; Hrouda, 1986; Borradaile and Geneviciene 2007). However, the observation that quartz *c*-axes are randomly distributed (see above) indicates that quartz has little effect on the orientation of the magnetic ellipsoid. Additionally, the predominance of the phyllosilicates as carriers of the AMS is corroborated by the low temperature curves and the positive bulk susceptibility value.

4.1.2. AMS (room and low T) parameters and orientation of the ellipsoid

The bulk magnetic susceptibility of the specimens ranges from 215 to −8 ($\times10^{-6}$) SI. We have selected 11 sites for the study of the AMS based on the value of the bulk susceptibility (K_m). The sites with very low magnetic susceptibility values do not produce sensible results. The average bulk susceptibility at room temperature shows low values, with a total average of about 40×10^{-6} SI. Only two sites (631-3, 629-1) have a K_m higher than 100×10^{-6} SI. These higher values can indicate some ferromagnetic content, which is corroborated with the measurement of magnetic susceptibility at low temperature (from 77 K to room temperature). Despite the low intensity of K_m, a well-defined magnetic ellipsoid axes distribution is observed in the selected 11 sites, confirming the applicability of the method in these rocks. The exclusive appearance of oblate ellipsoids (Fig. 4A) is, *a priori*, consistent with the magnetic fabric carried by phyllosilicates; these minerals possess an intrinsic and highly oblate anisotropy, with the k_{min} axis sub-parallel (no more than 9°) to the crystallographic *c*-axis, with the corresponding k_{max} and k_{int} axes parallel the plane and almost equal in magnitude (Tarling and Hrouda, 1993; Martín-Hernández and Hirt, 2003). The sites show different corrected anisotropy degrees (*P′*) for similar *T* values (Fig. 4B). The *P′* values are relatively high, varying from 1.2 to 1.35, whereas *T* values are more homogeneous, clustered around 0.6–0.8, except for three sites with lower values at around 0.3. The average of *T* is lower for these three sites because some samples within the site show prolate shapes (in 631-2 and 630-2), or the magnetic susceptibility ellipsoid has a nearly spherical shape (in 627-4) (see Flinn diagram, Fig. 4A). The magnetic data for each site are listed in Tables 1 and 2.

One way to quantify the relationship between strain and the AMS fabric is to control the degree of grouping of the different axes (k_{max} and k_{min}). Previous studies have used the degree of grouping of k_{min} axes to establish the degree of shortening in low-to-moderately deformed rocks (e.g., Housen et al., 1993; Parés et al., 1999; Parés and

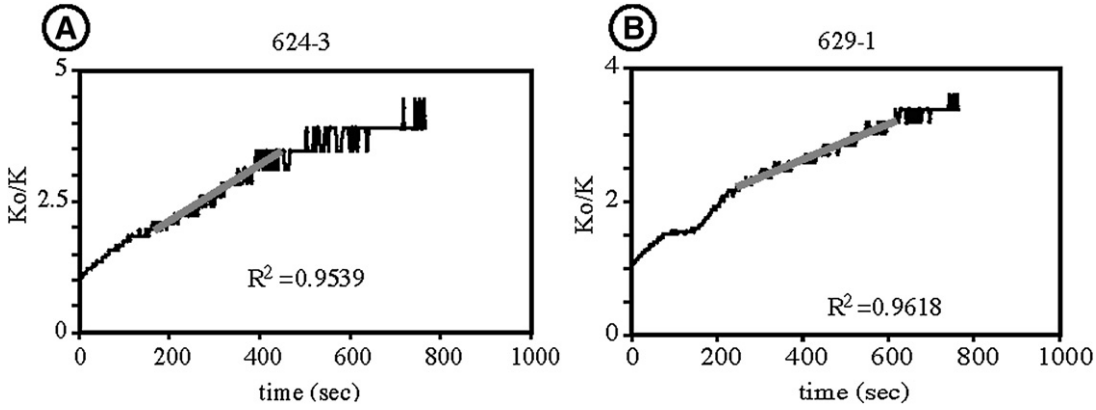

Fig. 3. Temperature dependence of low-field susceptibility for two samples, using the procedure of Richter and van der Pluijm (1994). K_o/K is the normalized reciprocal magnetic susceptibility. Regression line is calculated for *T* greater than 150 K (approximately) to exclude effects from the Verwey transition. A) The linear increase of the reciprocal susceptibility indicates that paramagnetic minerals dominate. This graph shows a predominance of paramagnetic carriers for the AMS. B) This graph shows some ferromagnetic influence at low temperature.

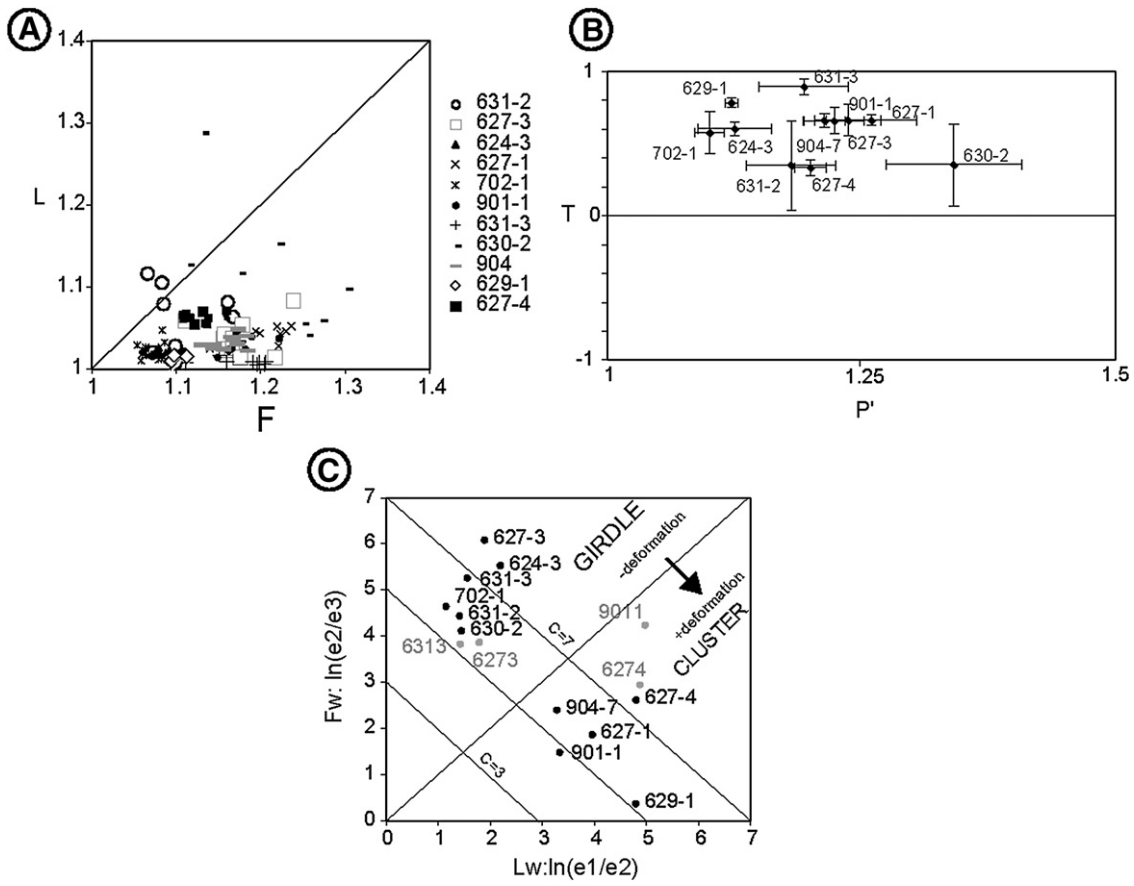

Fig. 4. A) The Flinn diagram for every sample. The magnetic lineation plots against the magnetic foliation. B) Diagram showing the variation of the corrected anisotropy degree (P') against the shape parameter (T, oblate in all samples) for each site with the standard deviation errors. C) Woodcock diagram for k_{max} axes (AMS) at room (black) and at low (grey) temperature. The grouping of k_{max} provides 3 eigenvalues derived from directional data. Two ratios of the three eigenvalues are plotted on a natural logarithmic scale. The ratios are L_w = Woodcock lineation ln (e1/e2) and F_w = Woodcock foliation ln (e2/e3) where e1>e2>e3.

van der Pluijm, 2004). Others have focused on the grouping of both axes maximum and minimum in low-to moderate deformed mudrocks to constrain the evolution of the fabric and the time of the acquisition of the AMS (Larrasoaña et al., 2004). Because the grouping of k_{min} axes is consistent in all of the Cretan samples, it cannot be used a proxy for the degree of strain evolution. Instead, the sites are separated using the grouping of k_{max} axes in the Woodcock diagram (Figs. 4C, 5 and 6). The Woodcock diagram is constructed with the eigenvalues of the k_{max} for every site, which will allow distinguishing gridle from cluster distributions of k_{max} axes (Fig. 4C).

The orientation of the AMS ellipsoid axes is shown in Fig. 5 and the bootstrap calculations and strain tensors are represented in Fig. 6. The k_{min} axes (and the minimum stretching axes, S_z) are always sub-vertical and perpendicular to the cleavage planes, which are nearly parallel to the sub-horizontal bedding planes; the k_{max} and k_{int} axes are distributed within a sub-horizontal plane. Most of k_{max} axes are NNE–SSW oriented. Site 631-3 is an exception, with the k_{int} axes oriented close to the N–S direction. This site has the highest T oblate value.

Table 2
τ_i are the eigenvalues and Dec. and inc. are the declination and inclination of the associated eigenvectors for the maximum (1), intermediate (2) and minimum (3) magnetic anisotropy axes (mapped to the lower-hemisphere). Matrix elements have been calculated from 15 measurements scheme, and the best-fit tensor elements were estimated using Tauxe's (1998) program.

Sample	τ 1	Dec.	Inc.	τ 2	Dec.	Inc.	τ 3	Dec.	Inc.
000624-3	0.3453	359	15.5	0.33959	95.6	22.4	0.31513	237.2	62.2
000627-1	0.3613	10.3	2.2	0.34606	280.3	2.3	0.29268	143	86.8
000627-3	0.3559	47.2	14.3	0.34952	316.9	0.9	0.29459	223.5	75.7
000627-4	0.3598	38.8	16.2	0.33918	130	4.1	0.30106	233.7	73.2
000629-1	0.3461	324.4	15.3	0.34221	59.5	18.1	0.31173	196.5	65.9
000630-2	0.3689	4.2	2.9	0.34357	100.4	7.8	0.28756	253.1	80.8
000631-2	0.3527	4.3	1.1	0.34142	94.5	6.2	0.30585	264	83.7
000631-3	0.3506	110.7	7.2	0.34896	19.9	1.9	0.30048	272.4	83.1
000702-1	0.3446	37	12.2	0.33992	131	18	0.31551	274.6	68
020901-1	0.3576	330.7	0.7	0.3458	60.9	14.2	0.2966	237.9	75.8
020904-7	0.3563	45.1	2	0.34572	136	17	0.29797	309.3	73.1

The bulk magnetic susceptibility at low temperature of the four selected sites ranges between 799 and 60.1×10^{-6} SI. The values are between 2.8 and 3.7 times the bulk magnetic susceptibility at room temperature (Fig. 7A). The increase of the bulk magnetic susceptibility values at low temperature reveals the presence of paramagnetic minerals. However, the sites in which the increase of the magnetic susceptibility at low temperature is less than 3.8 times and above 1 the value of the magnetic susceptibility at room temperature may contain either a partial contribution of ferromagnetic phases to the AMS or a paramagnetic phase with a paramagnetic Curie temperature above 0 K (chlorite and micas can have T_c around 30–35 K) (Lüneburg et al., 1999).

Nonetheless, the orientation of the axes at room and at low temperature overlaps in both group samples (Fig. 7B), indicating that the main contributors to the AMS at room temperature are the paramagnetic minerals (phyllosilicates).

4.2. Strain analysis

Strain results are shown in Table 3 and graphically in Fig. 6. The minimum stretching axis (S_z) is oriented sub-vertically, with a slight plunge towards the south. The intermediate and maximum extension axes are generally sub-horizontal, though the trends display significant variation because of the similarity in the values of S_x and S_y. The

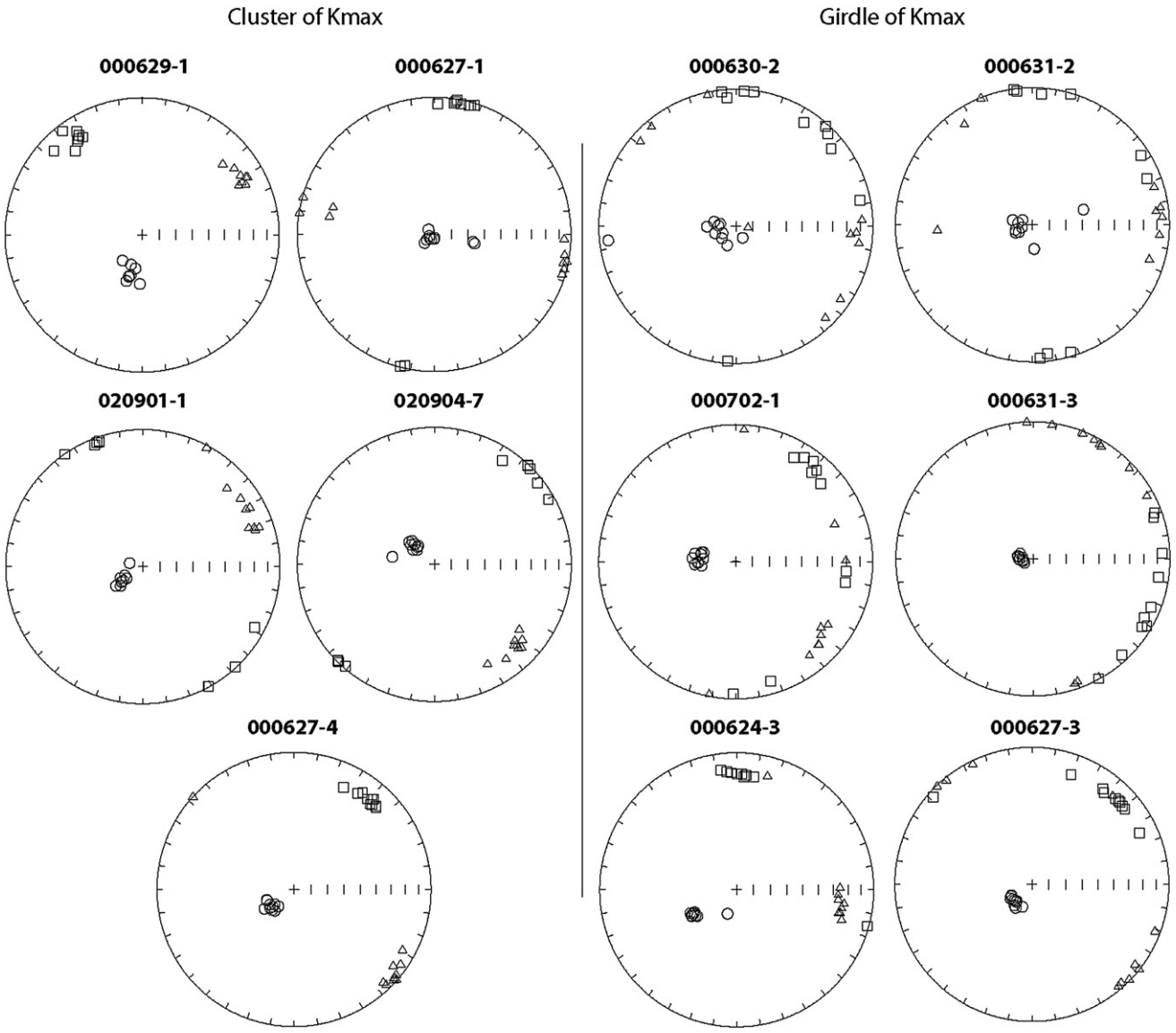

Fig. 5. Orientation of the AMS axes, squares: k_{max}, triangles: k_{int} and circles: k_{min}. Equal area lower-hemisphere projections. S_0 and S_1 are sub-horizontal.

shortening stretch, S_z, varies between 0.48 and 0.67, indicating a vertical shortening typically about 40%. For almost all samples the magnitude of the intermediate stretch, S_y, is larger than 1.0, indicating extension in multiple directions. The Flinn diagram (Fig. 8) indicates that the strain ellipsoids have a strong oblate geometry for most of the samples. The ductile strains are best characterized as a uniaxial flattening, with sub-vertical dissolution compensated by radial extension. The volume stretch, S_v, is typically about 25%, indicating that not all of the dissolved material was locally redeposited. Although some of this material was precipitated in veins that cut through bedding and in boudin necks, these features generally comprise only a few percent of outcrop exposures. This suggests that deformation must have been open-system on the scale of individual beds.

4.3. Preferred orientation of phylosilicates

Powder X-ray diffraction analysis (XRD) indicates that all 11 sites investigated contain varying amounts of phyllosilicate (mostly mica and some chlorite). The XTG measurements of both minerals show strong fabrics, suggesting that they formed under similar conditions. Eight of the eleven sites produced high to significantly high m.r.d. values ranging between 5.25 and 11.3; in the other sites phyllosilicates could not be detected by XTG. The samples with higher m.r.d. values display a prolate fabric, whereas samples with lower m.r.d. values show mainly oblate projections (Fig. 9A and B). Both types of fabrics occur in each samples group, with k_{max} in a girdle distribution and k_{max} in the cluster distribution.

A strong preferred orientation of these phyllosilicates (both mica and chlorite) is observed in the back-scattered electron (BSE) images (Fig. 9A and B). Both minerals vary in length and thickness in the different samples investigated. Whereas the mica in samples with a smaller m.r.d. are around 100 μm in length and 20–40 μm in thickness, significant long (in some cases more than 150 μm) and thin (less than 10 μm in thickness) mica minerals occur in samples with very high m.r.d., confirming mineral growth during solution mass-transfer. All mica minerals tend to be parallel to the cleavage planes.

5. Discussion

5.1. AMS and deformation: qualitative overlapping

The AMS ellipsoid within a cleavage domain is generally oriented with k_{min} axes well-grouped at the pole of the cleavage plane, whereas the k_{max} and k_{int} axes cluster within the cleavage plane. k_{max}

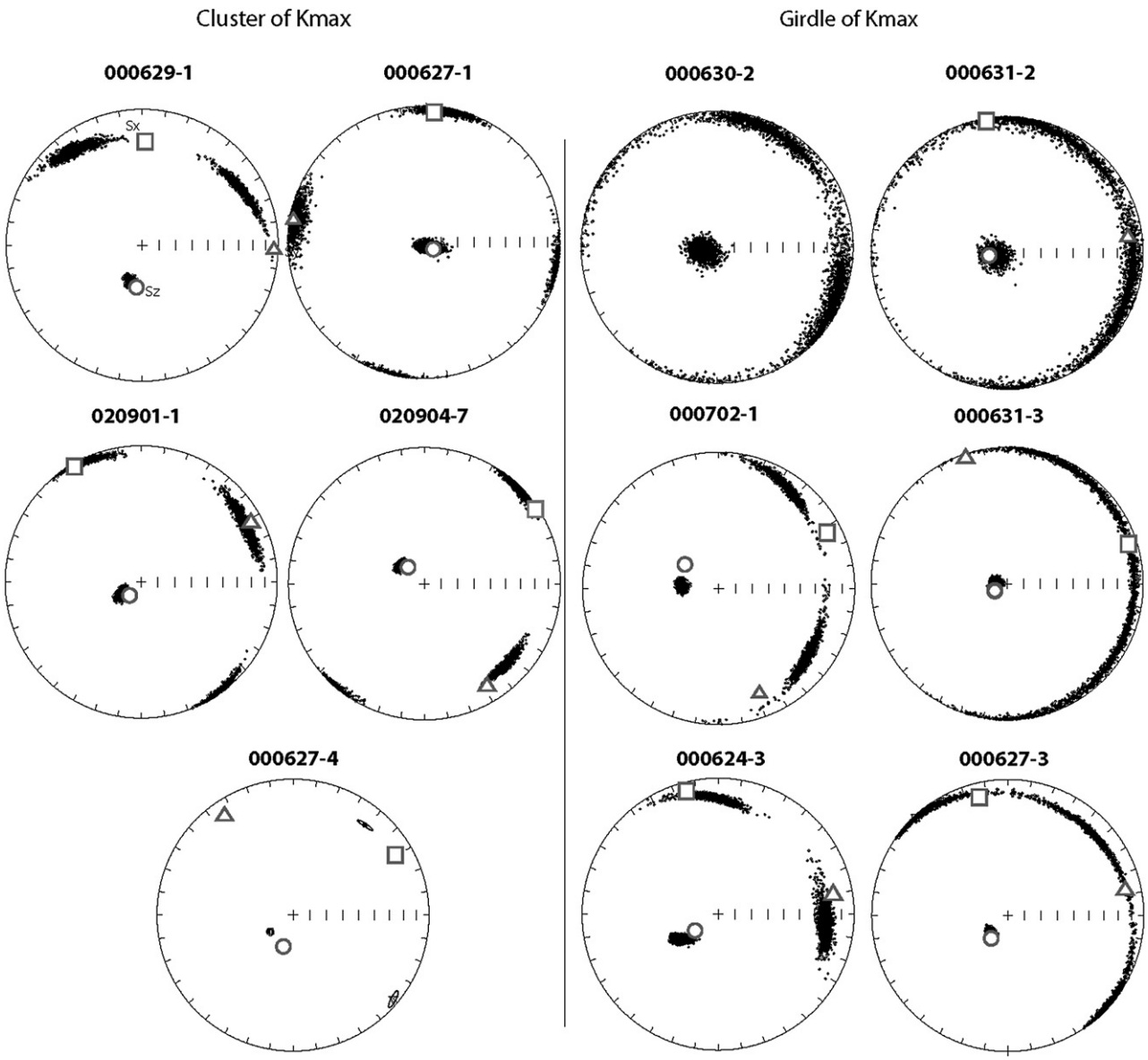

Fig. 6. Lower-hemisphere equal area projection of the corresponding bootstrapped eigenvectors calculated from the actual AMS data (black dots). Overlapping the bootstrap eigenvectors are the stretching axes calculated by the Projected Dimension Strain method: maximum: S_x (square), intermediate: S_y (triangle) and minimum: S_z (circle). The stretching axes are white with grey border symbols. The pole to the cleavage planes overlap with S_z.

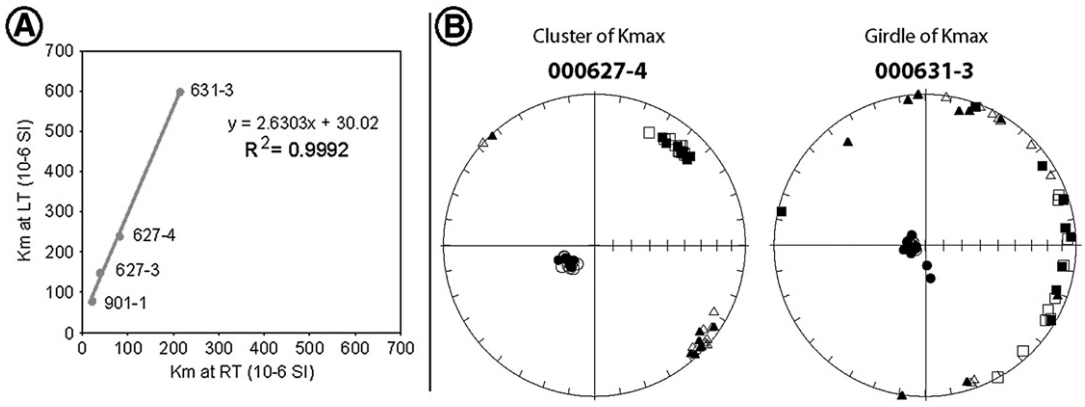

Fig. 7. A) Ratio of bulk susceptibility at low and room temperature of the four selected sites. B) Lower-hemisphere projection of the AMS axes at room (white) and low (black) temperature for both group of samples (cluster and girdle distribution of k_{max}).

Table 3
Strain axes and magnitudes (S_x, S_y, and S_z) from the projected dimension strain method. $S_v = S_x\ S_y\ S_z$.

Sample	Trend	Plunge	S_x	Trend	Plunge	S_y	Trend	Plunge	S_z	S_v
000624-3	348	08	1.29	080	12	1.26	226	76	0.63	1.02
000627-1	004	04	1.24	273	09	0.71	115	80	0.56	0.50
000627-3	345	12	1.35	078	13	1.13	213	72	0.44	0.67
000627-4	059	14	1.40	326	12	0.74	197	71	0.55	0.57
000629-1	001	25	1.37	092	03	1.20	188	64	0.48	0.78
000630-2	–	–	1.22	–	–	1.15	–	–	0.66	0.92
000631-2	082	11	1.21	352	00	1.16	260	80	0.62	0.86
000631-3	072	06	1.36	342	02	1.14	237	84	0.48	0.74
000702-1	063	11	1.14	157	20	1.14	307	66	0.63	0.82
020901-1	331	03	1.38	061	10	1.18	224	80	0.51	0.83
020904-7	057	03	1.24	148	14	1.13	315	76	0.49	0.69

is typically parallel to the elongation direction, which usually is the intersection of bedding and cleavage planes (L_1) (Singh et al., 1975; Kligfield et al., 1981; Hrouda, 1982; Borradaile, 1988; Aubourg et al., 1995; Borradaile and Henry, 1997; Parés et al., 1999; Aubourg et al., 2000; Parés and van der Pluijm, 2002). The AMS of the Crete samples shows the expected fabric, with k_{min} axes perpendicular to cleavage and k_{max} axes oriented in a NNE–SSW direction. Following Greiling (1982), the AMS fabrics has the same orientation of F1 (NE–SW) and F3 (N–S) structural lineation. The various magnetic lineations are coherent in the whole PQ unit and have formed parallel to the first-generation fold axes (Stöckhert et al., 1999). The folds are modified later by the pervasive sub-horizontal foliation and are consequently interpreted to form early in the deformation history, during the underplating process (Rahl, 2005). The trend of plate motion in the Hellenic subduction zone is also N-NE (Stöckhert et al., 1999; Bohnhoff et al., 2005).

The Phyllite–Quartzite rocks show a good correspondence between the orientation of the stretching axes or strain ellipsoid and the AMS ellipsoid axes (Fig. 6). The orientation of the finite strain axes generally overlaps with the magnetic fabric, although minor angular differences exist for three sites: 629-1, 702-1 and 627-3. The two first sites (629-1, 702-1) show some contribution of the ferromagnetic fraction (seen from low temperature curves, Fig. 3B) and hence the non-coaxiality could be a mineralogical (compositional) artifact since AMS shows the contribution of all minerals. Sample 629-1 has a lower degree of overlapping (35° difference) and the only one from the group of the k_{max} axes in a cluster distribution. The AMS of site 627-3 overlaps better with the strain ellipsoid if the k_{max} and k_{int} axes for AMS are transposed.

The k_{max} axes are consistently oriented NNE–SSW (Fig. 5), except for samples 629-1 and 901-1 from the clustered k_{max} group. In these sites the k_{max} axes have a NNW–SSE direction, although it is no more than 30° measured from north to west. The latter sample is the most oblate, and transposition between k_{max} and k_{int} (similar values) may occur.

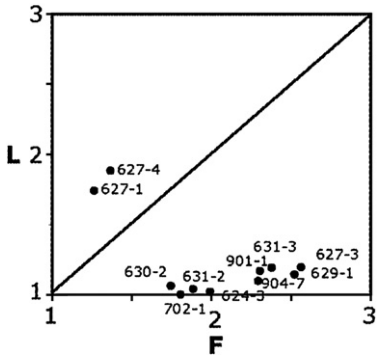

Fig. 8. Flinn diagram for the strain values (PDS method). $L = e1/e2$. $F = e2/e3$.

In thin-sections cut parallel to the cleavage plane, individual quartz grains show neither shape-preferred orientation nor evidence for dissolution. Instead, fibrous quartz–mica overgrowths developed during SMT deformation radiate outwards from the undeformed detrital quartz grains, indicating radial extension occurs in all directions within the foliation plane (Rahl, 2005). The lengths of the fibrous overgrowths do vary with direction, with the longest fibers generally oriented NNE–SSW. Thus, the elongation direction is similar to the orientation of the k_{max} axes in almost all cases. In addition, the elongation direction overlaps the macroscopically described stretching lineation, which is parallel to the first-generation of fold axes (Stöckhert et al., 1999).

The similarity of the AMS (phyllosilicates) and the strain (quartz) ellipsoids in these samples suggests that these features record the same deformational history. Since the quartz deformation record the SMT process, we infer the magnetic fabric is related to that process. This inference is supported by our observations of new mica growth during the SMT deformation (see Section 4.3). The fact that k_{max} axes seem to preserve the orientation of an early lineation parallel to macroscopic fold axes may indicate that SMT deformation did not totally obliterate the existing fabric or that the elongation direction maintains its orientation during the folding and dissolution–precipitation processes. The phyllosilicates show a prevalent orientation of k_{max} axes in the NNE–SSW direction. The paramagnetic fabric associated with the macrofolds is enhanced by the new crystallization of phyllosilicates within the microfibers of quartz during the formation of the flat-lying foliation (as observed by Rahl, 2005). The presence of phyllosilicates not only enhances SMT deformation (e.g., Marshak and Engelder, 1985) but also helps preserve the magnetic fabric, making this lithology appropriate for petrofabric studies in this particular tectonic setting.

5.2. Quantitative relationship

A long-standing goal of AMS studies is to establish a quantitative relationship between magnetic fabric and finite strain (Kneen, 1976; Wood et al., 1976; Rathore, 1979; Kligfield et al., 1981; Borradaile 1991; Hirt et al., 1993; Lüneburg et al., 1999; Parés and van der Pluijm, 2003). Previous work demonstrates that T shape is a fairly good indicator of evolution of fabric with increasing deformation in certain situations (e.g. in low-to moderately deformed mudrocks) (Joseph et al., 1998; Parés et al., 1999; Parés et al., 2001; Parés and van der Pluijm, 2003). However, in highly-strained rocks like in our study area, the development of a strong cleavage causes all samples to have similar T values that indicate a similar degree of preferred grain orientation.

In some studies (Parés et al., 1999; Larrasoaña et al., 2004), the fabric development is stronger with higher C values in the Woodcock diagram (Fig. 4C). Interestingly, most of the C values for our samples are between 5 and 7 (except 3 sites) in both groups. In addition, the samples remain in two groups at low temperatures, although there is an increase of the C values in the Woodcock diagram of the samples with k_{max} clustered, and a decrease of the C values for the samples

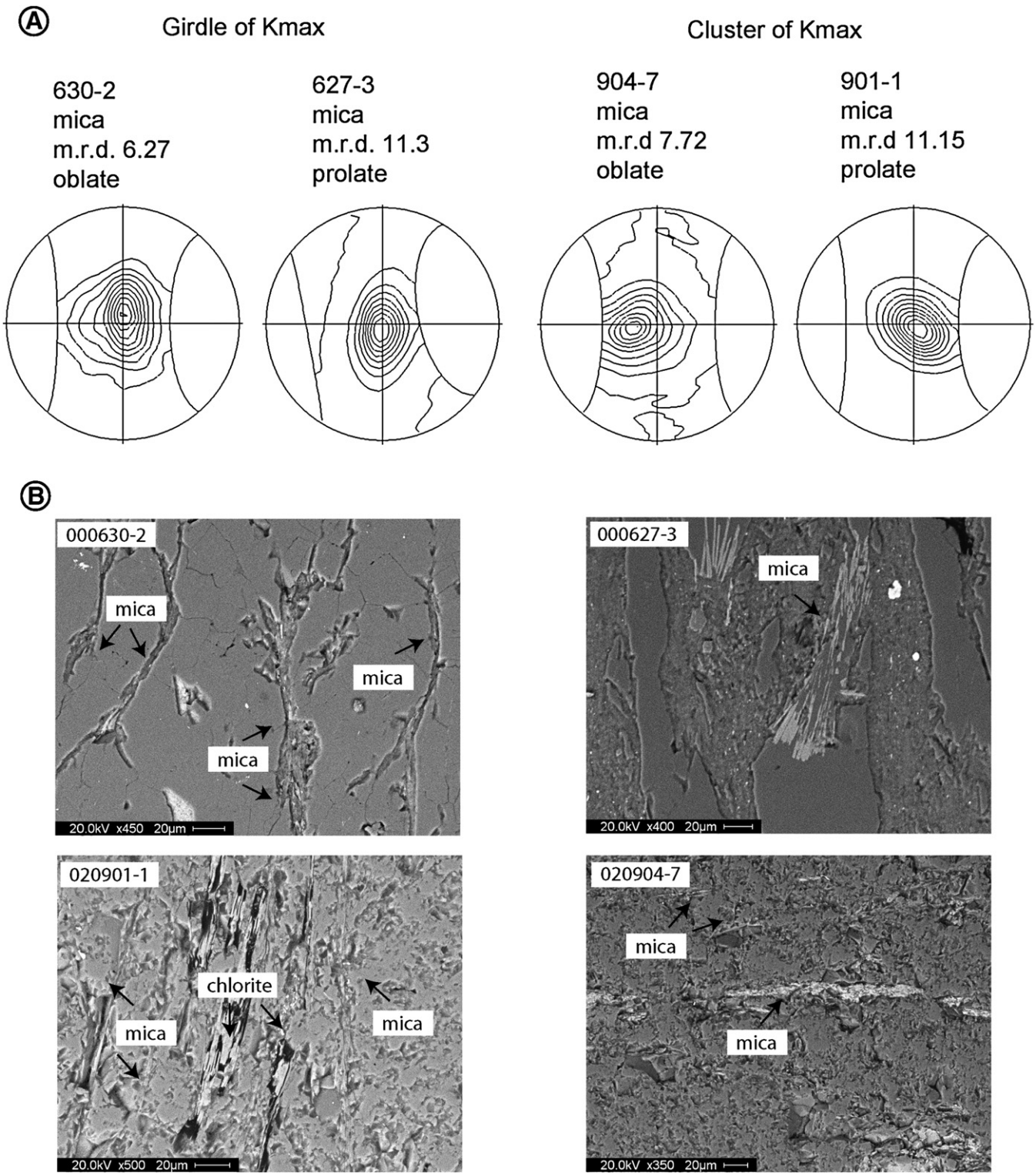

Fig. 9. A) XTG plots and SEM images of selected samples showing the variety of m.r.d. values in the girdle k_{max} axes distribution and in the cluster k_{max} axes distribution. B) SEM images of the samples in A.

with k_{max} in a gridle distribution (Fig. 4C). Consequently, we searched for a relationship between the strain and the grouping degree of k_{max} axes to confirm the use of the Woodcock diagram as an indicator of the strength of the magnetic fabric. The simplest relationship would show a higher clustering degree of k_{max} axes (higher L_w and C) as strain increases, as seen in the evolution from a sedimentary fabric to a strongly cleaved one (Parés et al., 1999). A first observation when comparing S_x and S_z values with L_w and F_w (Fig. 10) is an increase of S_x with increasing L_w or F_w for both groups of samples (except for two sites in the cluster group, which show similar S_x values as some of the girdle group). The increase of S_x values in the girdled group is more dramatic than for the clustered group (Fig. 10A and B). This indicates that stretching values in the X direction are more determinative for the girdle group. It is the opposite for the S_z values, since the clustered

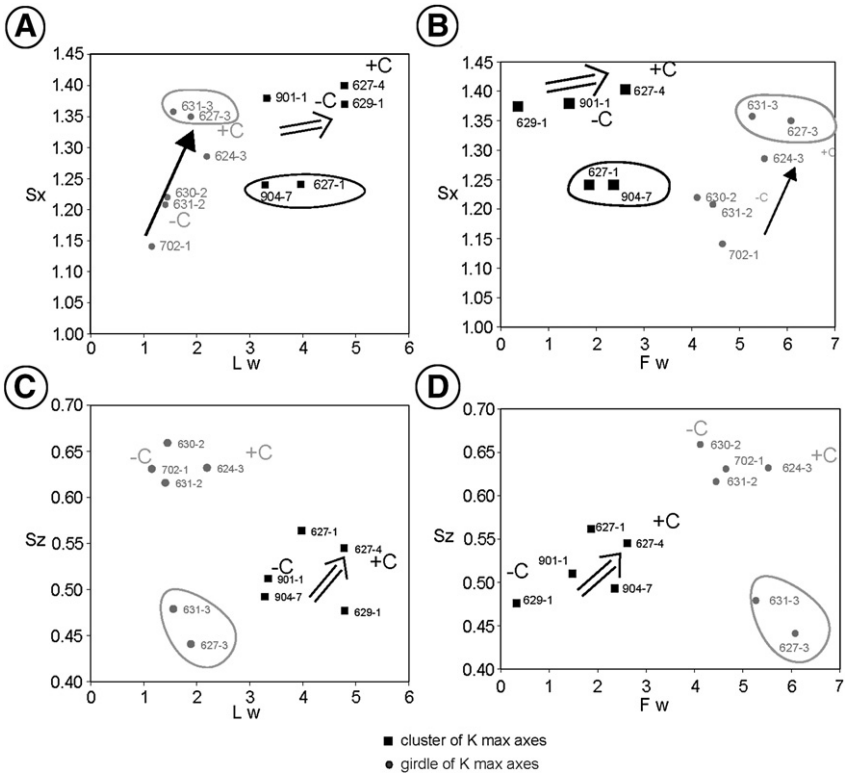

Fig. 10. Diagrams showing the change of S_x and S_z with L_w and F_w for girdled and clustered samples, *C* values from Woodcock diagram are represented qualitatively. A) S_x/L_w where girdled samples are better differentiated with S_x. B) S_x/F_w diagram shows a similar pattern as in A. C) S_z/L_w diagram where the evolution of girdled samples with strain is better characterized. D) S_z/F_w diagram, similar to C.

samples show a better correspondence with S_z, especially in the S_z/F_w diagram (Fig. 10C and D). The S_z values are lower for the clustered group but characterize better the evolution of the fabric with the strain. The S_z values are the highest and very similar for the girdled samples except for two samples (631-3 and 627-3), one of which is the most oblate shaped one (631-3). S_z is higher for higher values of L_w and F_w in the clustered samples. The relationship between the strain and the grouping of the k_{max} cannot be directly inferred from the Woodcock and has to be careful considered; however, the lower values of L_w correlate with S_x (the maximum stretching value) and lower values of F_w correlate better with S_z (the minimum stretching value).

The absolute values of the axes of the ellipsoids are apparently not comparable since the eigenvalues of $\tau 1$, $\tau 2$ and $\tau 3$ barely change within the sites (a range of 0.03 U). In contrast, the strain magnitudes (S_x, S_y and S_z) show greater variation (0.4 U). The relationship of the absolute values of the eigenvalues obtained from the AMS ellipsoid and the tensor values from the strain ellipsoid for each site has been used to quantify the magnetic susceptibility ellipsoid evolution with respect to the stretching magnitudes as in Kligfield et al. (1981) and Lüneburg et al. (1999). It reflects the changes in the magnetic fabric due to the increase in the absolute values of strain. In the *Y* axis *M* is plotted ($M=(K_i-K)/K$, where K_i for one sample is the normed principal susceptibility value of k_{max}, k_{int} or k_{min} multiplied by the norming factor and *K* is the average of all three principal susceptibility values) and in the *X* axes are the values of stretching tensor in logarithmic values (log Si). A linear relationship is established, although some scatter is present (Fig. 11). This function relates directly and quantitatively the changes in the anisotropy with the changes in the stretching values. A line passing through the center would imply a high correlation between the strain and the magnetic fabric response to strain. In these phyllites from Crete the relationship is linear with a moderate correlation degree ($R^2=0.7$), but the line does not cross the center of the axes (0.0). This implies that a pre-existing fabric was present when the SMT strain developed (when log Si = 0, there is certain fabric imposed, since *M* is not 0). This observed linear correlation may reflect the inheritance of the "folding" fabric in the "SMT" fabric, although this relationship can be used only at very local scale (as seen in Kligfield et al., 1981). The moderate correlation between AMS and strain tensor is elusive, probably due to the new formation of phyllosilicates during the two main deformation processes: folding and SMT.

Finally, the strength in the stacking of the octahedral layers of phylloslicates (m.r.d. values) correlates well with S_x in the clustered k_{max} axes fabrics. However the correlation of m.r.d and S_x is unclear in the girdle type of AMS fabrics: some low m.r.d values correspond to samples with high S_x eigenvalues, probably due to the competing effect of the girdle distribution (micas oriented radially in the cleavage plane). In any case, the prolate shapes of the XTG plots are related to stronger fabric (higher m.r.d.).

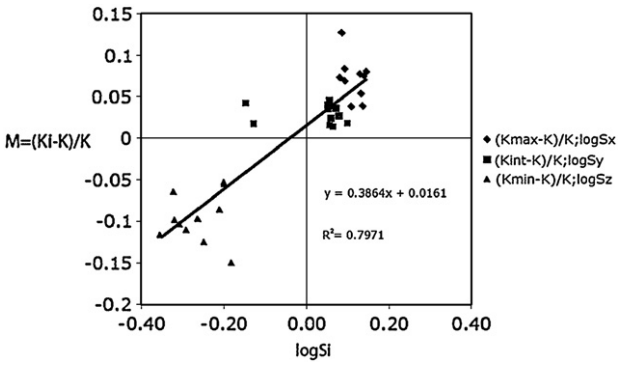

Fig. 11. Mean values for each site of *M* against log Si (Si = stretching values) with the calculated linear relationship.

6. Conclusions

The study of phyllites from Crete allows a comparison of the magnetic fabrics at room and low temperature with strain. In addition, the stacking of the octahedral layers of phylloslicates is controlled by XTG. The different methods, each sensitive to different minerals, are used to investigate the development of a petrofabric in a complex structural setting. From our data we conclude:

(1) A qualitative correlation exists between the orientation of the magnetic (at room and low temperature) and strain ellipsoids. In both cases, the minimum axes (k_{min} and S_z) are nearly vertical and the maximum axes (k_{max} and S_x) overlap in a NNE–SSW direction.
(2) The NNE–SSW direction is related to a fabric that pre-dates the development of a SMT fabric. The earlier fabric is related to the macroscopic stretching direction (NNE–SSW) that aligns with fold axes. Subsequent dissolution–precipitation developed with an elongation direction parallel to the pre-existing fold axes.
(3) The quantitative relationship between AMS and strain is elusive, probably due to the different processes that affect quartz (dissolution and precipitation) and phyllosilicates (recrystallization). Nevertheless, a weak correlation is discovered between the strain values in S_x and S_z axes with the grouping of k_{max} in both types of groups. Girdled samples evolve with S_x and clustered fabric with S_z values.
(4) The Woodcock diagram for the grouping of k_{max} has to be carefully considered in order to correlate with the strain.
(5) The m.r.d. XTG values correlates with the strain in the clustered type of AMS fabrics. This relationship is unclear in the girdle AMS fabrics.

Acknowledgements

B.O.U. thanks a postdoctoral grant and Juan de la Cierva Program together with the projects CGL2006-05817 and CGL2009-08969 from MEC-MSI (Spain) and the Sokol postdoctoral award from the University of Michigan (U. of M.). Rob van der Voo and Rod C. Ewing from the Department of the Geological Sciences of the U. of M. are fully acknowledged for their support. J.M.R. was supported by a Turner Post-doctoral Fellowship from the University of Michigan. Ben van der Pluijm (U. of M.) is also acknowledged for fruitful discussions. We also thank the assistance from the EMAL laboratory staff at the University of Michigan. We acknowledge the careful revisions of B. Almqvist and one anonymous reviewer.

References

Anderson, M.W., Morris, A., 2004. The puzzle of axis-normal magnetic lineations in folded low-grade sediments (Bude Formation, SW England). In: Martín-Hernández, F., Lüneburg, C.M., Aubourg, C., Jackson, M. (Eds.), Magnetic Fabric; Methods and Applications: Geological Sciety special Publication, 238, pp. 175–190.

Angelier, J., Barrier, E., Huchon, P., 1982. Sur les relations entre trajectoires de contrainte et directions de mouvement le long d'une frontiere convergente; exemples de la subduction hellenique (Grece) et de la collision Philippines–Eurasie (Taiwan et Japon). Translated Title: Relationship between strain trajectories and movement directions along a converging front; Hellenic subduction in Greece, and Philippines–Eurasia plate collision in Taiwan and Japan. Comptes-Rendus des Seances de l'Academie des Sciences, Serie 2: Mecanique-Physique, Chimie, Sciences de l'Univers, Sciences de la Terre. 294 (12), 745–748.

Aubourg, C., Chabert-Pelline, C., 1999. Neogene remagnetization of normal polarity in the Late Jurassic black shales from the southern Subalpine Chains (French Alps). Evidence for anticlockwise rotations. Tectonophyscis 308, 437–486.

Aubourg, C., Rochette, P., Bergmüller, F., 1995. Composite magnetic fabric in weakly deformed black shales. Physics of the Earth and Planetary Interiors 87, 267–278.

Aubourg, C., Frizon de Lamotte, D., Poisson, A., Mercier, E., 1997. Magnetic fabrics and oblique ramp-related folding: a case study from the western Taurus (Turkey). Journal of Structural Geology 19 (8), 1111–1120.

Aubourg, C., Rochette, P., Stéphan, J.F., Popoff, M., 1999. The magnetic fabric of weakly deformed Late Jurassic shales from the southern subalpines chains (French Alps): evidence for SW-directed tectonic transport direction. Tectonophysics 307, 15–31.

Aubourg, C., Hebert, R., Jolivet, L., Cartayrade, G., 2000. The magnetic fabric of metasediments in a detachment shear zone: the example of Tinos Island (Greece). Tectonophysics 321, 219–236.

Averbuch, O., Mattei, M., Kissel, C., Frizon de Lamotte, D., Speranza, F., 1995. Cinématique des déformations au sein d'un système chevauchant aveugle: l'exemple de la "Montagna dei Fiori" (front des Apenins centraux, Italie). Bulletin de la Société Géologique de France 5, 451–461.

Bohnhoff, M., Harjes, H.-P., Meier, T., 2005. Deformation and stress regimes at the Hellenic subduction zone from focal mechanisms. Journal of Seismology 9 (3), 341–366.

Borradaile, G.J., 1987. Anisotropy of magnetic susceptibility: rock composition versus strain. Tectonophysics 138, 327–329.

Borradaile, G.J., 1988. Integration of rock magnetic and rock deformation studies. 23rd General Assembly of the European Geophysical Society; Part I, Society Symposia, Solid Earth, Geophysics and Geodesy: Annales Geophysicae, 16 (1), p. 197.

Borradaile, G.J., 1991. Correlation of strain with anisotropy of magnetic susceptibility (AMS). Pure and Applied Geophysics 135, 15–29.

Borradaile, G., Geneviciene, I., 2007. A case of time-dependent anisotropy of low-field susceptibility (AMS). Physics of the Earth and Planetary Interiors 162, 227–243.

Borradaile, G.J., Henry, B., 1997. Tectonic applications of magnetic susceptibility and its anisotropy. Earth Science Reviews 42, 49–93.

Borradaile, G.J., Jackson, M., 2004. Anisotropy of magnetic susceptibility (AMS): magnetic petrofabrics of deformed rocks. In: Martín-Hernández, F., Lüneburg, C.M., Aubourg, C., Jackson, M. (Eds.), Magnetic Fabric, Methods and Applications: Geological Society Special Publication, 238, pp. 299–360.

Borradaile, G.J., Sarvas, P., 1990. Magnetic susceptibility fabrics in slates, structural, mineralogical, and lithological influences. Tectonophysics 172, 215–222.

Borradaile, G.J., Tarling, D.H., 1981. The influence of deformation mechanisms on magnetic fabrics in weakly deformed rocks. Tectonophysics 77, 151–168.

Debacker, T.N., Robion, P., Sintubin, M., 2004. The anisotropy of magnetic susceptibility (AMS) in low-grade, cleaved pelitic rocks: influence of cleavage/bedding angle and type and relative orientation of magnetic carriers. In: Martín-Hernández, F., Lüneburg, C.M., Aubourg, C., Jackson, M. (Eds.), Magnetic Fabric, Methods and Applications: Geological Sciety special Publication, 238, pp. 77–108.

Dornsiepen, U.F., Manutsoglu, E., Mertmann, D., 2001. Permian–Triassic palaeogeography of the external Hellenides. Palaeogeography, Palaeoclimatology, Palaeoecology 172 (3–4), 327–338.

Fassoulas, C., Kilias, A., Mountrakis, D., 1994. Postnappe stacking extension and exhumation of high-pressure/ low-temperature rocks in the Island of Crete, Greece. Tectonics 13 (1), 125–138.

Feehan, J.G., Brandon, M.T., 1999. Contribution of ductile flow to exhumation of low-temperature, high-pressure metamorphic rocks; San Juan–Cascade nappes, NW Washington State. Journal of Geophysical Research, B, Solid Earth and Planets 104 (5), 10,883–10,902.

Goldstein, A.G., 1980. Magnetic susceptibility anisotropy of mylonites from the Lake Char mylonite zone, southeastern New England. In: Schwerdtner, W.M., Hudleston, P.J., Dixon, J.M. (Eds.), Analytical Studies in Structural Geology: Tectonophysics, 66, pp. 197–211. 1–3.

Graham, J.W., 1954. Magnetic susceptibility anisotropy, an unexploited petrofabric element. Geological Society of America Bulletin 1257–1258 65; 12 (2).

Graham, J.W., 1966. Significance of magnetic anisotrophy in Appalachian sedimentary rocks. The Earth Beneath the Continents—A Volume of Geophysical Studies in Honor of Merle A. Tuve: Geophysical Monograph, pp. 627–648.

Greiling, R., 1982. The metamorphic and structural evolution of the Phyllite–Quartzite Nappe of western Crete. Journal of Structural Geology 4 (3), 291–297.

Henry, B., Daly, L., 1983. From qualitative to quantitative magnetic anisotropy analysis; the prospect of finite strain calibration. Tectonophysics 98 (3–4), 327–336.

Hirt, A.M., Lowrie, W., Clendenen, W.S., Kligfield, R., 1988. The correlation of magnetic anisotropy with strain in the Chelmsford Formation of the Sudbury Basin, Ontario. Tectonophysics 145 (3–4), 177–189.

Hirt, A.M., Lowrie, W., Clendenen, W.S., Kligfield, R., 1993. Correlation of strain and the anisotropy of magnetic susceptibility in the Onaping Formation: evidence for a near-circular origin of the Sudbury Basin. Tectonophysics 225, 231–254.

Hirt, A.M., Lowrie, W., Lüneburg, C.M., Lebit, H., Engelder, T., 2004. Magnetic and mineral fabric development in the Ordovician Martinsburg Formation in the Central Appalachian fold and thrust belt, Pennsylvania. In: Martin-Hernandez, F., Lueneburg, C.M., Aubourg, C., Jackson, M. (Eds.), Magnetic Fabric; Methods and Applications: Geological Society Special Publications, 238, pp. 109–126.

Housen, B.A., van der Pluijm, B., 1990. Chlorite control of correlations between strain and anisotropy of magnetic susceptibility. Physics of the Earth and Planetary Interiors 13, 315–323.

Housen, B.A., Richter, C., van der Pluijm, B.A., 1993. Composite magnetic anisotropy fabrics: experiments, numerical models, and implications for the quantification of rock fabrics. Tectonophysics 220, 1–12.

Housen, B.A., van der Pluijm, B., Essene, E.J., 1995. Plastic behavior of magnetite and high strains obtained from magmatic fabrics in the Parry Sound shear zone, Ontario Grenville Province. Journal of Structural Geology 17 (2), 265–278.

Hrouda, F., 1982. Magnetic anisotropy of rocks and its application in geology and geophysics. Geophysical Surveys 5, 37–82.

Hrouda, F., 1986. The effect of quartz on the magnetic-anisotropy of quartzite. Studia Geophysica et Geodaetica 30, 39–45.

Hrouda, F., 1987. Mathematical model relationship between the paramagnetic anisotropy and strain in slates. Tectonophysics 142 (2–4), 323–327.

Jackson, M., 1991. Anisotropy of magnetic remanence: a brief review of mineralogical sources, physical origins, and geological applications, and comparison with susceptibility anisotropy. Pure and Applied Geophysics 136, 1–28.

Jackson, M., Tauxe, L., 1991. Anisotropy of magnetic susceptibility and remanence: developments in the characterization of tectonic, sedimentary, and igneous fabric. Geophysical Research Letters 29, 371–376.
Jelinek, V., 1978. Statistical processing of anisotropy of magnetic susceptibility measured on groups of specimens. Studia Geophysica et Geodaetica 22, 50–62.
Jelinek, V., 1981. Characterization of the magnetic fabric of rocks. Tectonophysics 79 (3–4), T63–T67.
Jolivet, L., Goffe, B., Monie, P., Truffert, L.C., Patriat, M., Bonneau, M., 1996. Miocene detachment in Crete and exhumation *P–T–t* paths of high-pressure metamorphic rocks. Tectonics 15 (6), 1129–1153.
Joseph, L.H., Rea, D.K., van der Pluijm, B.A., 1998. Use of grain size and magnetic fabric analyses to distinguish among depositional environments. Paleoceanography 13, 491–501.
Kligfield, R., Lowrie, W., Dalziel, I.W.D., 1977. Magnetic susceptibility anisotropy as a strain indicator in the Sudbury Basin, Ontario. Tectonophysics 40 (3–4), 287–308.
Kligfield, R., Owens, W.H., Lowrie, W., 1981. Magnetic susceptibility anisotropy, strain and progressive deformation in Permian sediments from the Maritime Alps (France). Earth and Planetary Sciences Letters 55, 181–189.
Kligfield, R.W., Lowrie, W., Pfiffner, O.A., 1982. Magnetic properties of deformed oolitic limestones from the Swiss Alps: the correlation of magnetic anisotropy and strain. Eclogea Geologica Helvetica Acta 75, 127–157.
Kneen, S., 1976. The relationship between the magnetic and strain fabrics of some haematite-bearing. Welsh, slates. Earth and Planetary Earth Sciences 31, 413–416.
Krahl, J., Kaufmann, G., Kozur, H., Richter, D., Foerster, O., Henritzi, F., 1983. Neue Daten zur Biostratigraphie und zur tektonischen Lagerung der Phyllit-Gruppe und der Trypali-Gruppe auf der Insel Kreta (Griechenland). Translated Title: New data on the biostratigraphy and tectonics of the Phyllades Group and the Trypali Group in Crete, Greece. Geologische Rundschau 72 (3), 1147–1166.
Larrasoaña, J.C., Pueyo, E.L., Parés, J.M., 2004. An integrated AMS structural, paleo- and rock-magnetic study of the Eocene marine marls from the Jaca–Pamplona basin (Pyrenees, N Spain); new insights into the timing of magnetic fabric acquisition in weakly deformed mudrocks. In: Martín-Hernández, F., Lüneburg, C.M., Aubourg, C., Jackson, M. (Eds.), Magnetic Fabric, Methods and Applications: Geological Society special Publication, 238, pp. 127–143.
Le Pichon, X., Angelier, J., 1981. The Aegean Sea. In: Extensional tectonics associated with convergent plate boundaries. In: Vine, F.J., Smith, A.G. (Eds.), Conveners: Philosophical Transactions of the Royal Society of London, Series A: Mathematical and Physical Sciences, 300(1454), pp. 357–372.
Lowrie, W., 1989. Magnetic analysis of rock fabric. In: James, D.E. (Ed.), The Encyclopedia of Solid Earth Geophysics. Van Nostrand Reinhold. Princeton, New Jersey, pp. 698–706.
Lüneburg, C.M., Lampert, S.A., Lebit, H.D., Hirt, A.M., Casey, M., Lowrie, W., 1999. Magnetic anisotropy, rock fabrics and finite strain in deformed sediments of SW Sardinia (Italy). Tectonophysics 307, 51–74.
Marshak, S., Engelder, T., 1985. Depelopment of cleavage in limestones of a fold–thrust belt in eastern New York. Journal of Structural Geology 7 (374), 345–359.
Martín-Hernández, F., Hirt, A.M., 2003. The anisotropy of magnetic susceptibility in biotite, muscovite and chlorite single crystals. Tectonophysics 367, 13–28.
Nye, J.F., 1957. Physical properties of crystals. Claredon Press, Oxford. 322 pp.
Parés, J.M., van der Pluijm, B.A., 2002. Evaluating magnetic lineations (AMS) in deformed rocks. Tectonophysics 350, 283–298.
Parés, J.M., van der Pluijm, B.A., 2003. Magnetic fabrics and strain in pencil structures of the Knobs Formation, Valley and Ridge Province, US Appalachians. Journal of Structural Geology 25, 1349–1358.
Parés, J.M., van der Pluijm, B.A., 2004. Correlating magnetic fabrics with finite strain; comparing results from mudrocks in the Variscan and Aappalachian orogens. Geologica Acta 2 (3), 213–220.
Parés, J.M., van der Pluijm, B., Dinarès-Turell, J., 1999. Evolution of magnetic fabrics during incipient deformation of mudrocks (Pyrenees, northern Spain). Tectonophysics 307, 1–14.
Parés, J.M., van der Pluijm, B., Cirès, J., 2001. Tectonic Lineation and Magnetic Fabrics in Deformed Rocks, GSAAnnual Meeting, Boston, MA.
Rahl, J.M., 2005. Tectonic evolution of the Hellenic (Greece) and Otago (New Zealand) subduction wedges, Ph.D. thesis, Yale University, 208 pp.
Rahl, J.M., Anderson, K.M., Brandon, M.T., Fassoulas, C., 2005. Raman spectroscopic carbonaceous material thermometry of low-grade metamorphic rocks: calibration and application to tectonic exhumation in Crete, Greece. Earth & Planetary Science Letters 240, 339–354.
Rathore, J.S., 1979. Magnetic susceptibility anisotropy in the Cambrian slate belt of North Wales and correlation with strain. Tectonophysics 53, 83–97.
Rathore, J.S., 1980. Magnetic susceptibility anisotropy from the Borrowdale Volcanic Group in the English Lake District and their correlation with strain. Tectonophysics 57, 207–220.
Rathore, J.S., Henry, B., 1982. Comparison of strain and magnetic fabrics in Dalradian rocks from the Southwest Highlands of Scotland. Journal of Structural Geology 4 (3), 373–384.
Rees, A.I., 1965. The use of anisotropy of magnetic susceptibility in the estimation of sedimentary fabric. Sedimentology 4 (4), 257–271.
Richter, C., van der Pluijm, B.A., 1994. Separation of paramagnetic and ferrimagnetic susceptibilities using low temperature magnetic susceptibilities and comparison with high field methods. Physics of the Earth and Planetary Interiors 82 (2), 113–123.
Ring, U., Brandon, M.T., 1999. Rheology and stability of accretionary wedges; an example from the Franciscan Complex, USA. In: Dietrich, P.G., Franke, W., Merkel, B.J., Herzig, P. (Eds.), 89th Annual Meeting of the Geologische Vereinigung; Old crust, New Problems; Geodynamics and utilization; Abstracts and Programme; Includes the Final International Colloquium of the DFG Priority Programme "Orogenic Processes; Quantification and Modeling in the Variscan Belt". Terra Nostra (Bonn). 99-1, 168.
Rochette, P., 1987. Magnetic susceptibility of the rock matrix related to magnetic fabric studies. Journal of Structural Geology 9, 1015–1020.
Rochette, P., Jackson, M., Aubourg, C., 1992. Rock magnetism and the interpretation of anisotropy of magnetic susceptibility. Reviews of Geophysics 30, 209–226.
Schwarz, S., Stöckhert, B., 1996. Pressure solution in siliciclastic HP–LT metamorphic rocks; constraints on the state of stress in deep levels of accretionary complexes. In: Stel, H. (Ed.), Paleostress analysis; a tool in structural geology: Tectonophysics, 255 (3–4, pp. 203–209.
Singh, J., Sanderson, D.J., Tarling, D.H., 1975. The magnetic susceptibility anisotropy of deformed rocks from North Cornwall, England. Tectonophysics 27, 141–153.
Stöckhert, B., Wachmann, M., Kuester, M., Bimmermann, S., 1999. Low effective viscosity during high pressure metamorphism due to dissolution precipitation creep; the record of HP–LT metamorphic carbonates and siliciclastic rocks from Crete. In: Schmid, S.M., Heilbronner, R., Holger, S. (Eds.), Deformation mechanisms in nature and experiment: Tectonophysics, 303(1–4), pp. 299–319.
Tarling, D.H., Hrouda, F., 1993. The Magnetic Anisotropy of Rocks. Chapman and Hall, London.
Tauxe, L., 1998. Paleomagnetic principles and practice. Modern Approaches in Geophysics. 18. Kluwer Academic Publishers. 299 pp.
Theye, T., Seibel, E., Vidal, O., 1992. Carpholite, sudoite, and chloritoid in low-grade high-pressure metapelites from Crete and the Peloponnese, Greece. European Journal of Mineralogy 4 (3), 487–507.
Van der Pluijm, B.A., Ho, N.-C., Peacor, D., 1994. High-resolution X-ray texture goniometry. Journal of Structural Geology 16 (7), 1029–1032.
Wenk, H.R., 1985. Measurement of pole figures. In: Wenk, H.R. (Ed.), Preferred Orientation in Deformed Metals and Rocks; An Introduction to Modern Texture Analysis, pp. 11–47.
Wood, D.S., Oertel, G., Singh, J., Benett, H.F., 1976. Strain and anisotropy in rocks. Philosophical Transactions of the Royal Society of London, Serie A 283, 27–42.
Woodcock, N.H., 1977. Specification of fabric shapes using an eigenvalue method. Geological Society of America Bulletin 88 (9), 1231–1236.